# Dynamical behavior of spots in a nonequilibrium distributive active medium

F.-J. Niedernostheide, M. Or-Guil, M. Kleinkes, and H.-G. Purwins
*Institut für Angewandte Physik, Universität Münster, Corrensstraße 2/4, D-48149 Münster, Germany*
(Received 26 November 1996)

Numerical studies of a two-dimensional active medium with long-range inhibition and additional global inhibition far from equilibrium, show a bifurcation sequence from stationary spots to elliptically oscillating spots, followed by a transition to traveling spots. General properties of the spot dynamics and their dependence on the applied boundary conditions, as well as on the global inhibition are discussed. [S1063-651X(97)11104-7]

PACS number(s): 05.70.Ln, 72.20.−i, 85.30.−z, 82.20.Wt

## I. INTRODUCTION

Standing and moving localized particlelike structures in two-dimensional systems have been experimentally observed, e.g., in chemical systems [1,2], in gas discharges [3,4], and semiconductor materials [5] and have been successfully described in terms of reaction-diffusion equations of an activator inhibitor type. The stability of spots on a two-dimensional domain with respect to breathing and static deformations has been studied for simple piecewise linear activator kinetics [6]. In recent studies [7–9] collisions of traveling spots have been investigated numerically in extended two-dimensional media, and an asymptotic method for describing instabilities of spots in two and three dimensions has been presented [10].

The aim of the present paper is to investigate the behavior of two-dimensional spots upon variation of a parameter that drives the system far from equilibrium. We shall devote special attention to the influence of the boundary conditions and a nonlocal inhibition. For that purpose we consider the two-dimensional equivalent of the two-component set of reaction-diffusion equations that has been derived [11], and successfully applied [12], to explain the experimentally observed dynamics and bifurcation behavior of current-density filaments in a quasi-one-dimensional silicon multilayered $p^+$-$n^+$-$p$-$n^-$ device.

## II. MODEL EQUATIONS

First we briefly describe the model equations and recapitulate the relevant physical mechanisms the model is based on: The $p^+$-$n^+$-$p$-$n^-$ device is considered to be composed of two parts, a $p^+$-$n^+$-$p$ transistor and a $p$-$n^-$ diode. Treating the transistor as an avalanche transistor which is coupled to a Shockley diode, the following two-component set of reaction-diffusion equations can be derived [11]:

$$\frac{\partial V_e}{\partial t} = D_e \Delta V_e - q(V_e, p), \tag{1}$$

$$\frac{\partial p}{\partial t} = D_p \Delta p + Q(V_e, p), \tag{2}$$

where $V_e$ is the voltage drop across the $p^+$-$n^+$ junction of the transistor and represents the activator, while $p$ denotes the average hole density in the $n^-$ layer of the diode part and acts as an inhibitor. The diffusion coefficient $D_e = w\sigma_b / C_e$ is determined by the capacity $C_e$ of the $p^+$-$n^+$ junction and the width $w$ and conductivity $\sigma_b$ of the $n^+$ base. $D_p$ is the diffusion coefficient of holes in the $n^-$ layer. $\Delta$ denotes the Laplace operator in two space dimensions perpendicular to the main current flow direction. The reaction terms $q(V_e, p)$ and $Q(V_e, p)$ are determined by the current transport processes that are described in detail in Refs. [11,12]:

$$q(V_e, p) = \frac{1}{C_e}[j_e(V_e) - j_c(V_e, p)], \tag{3}$$

$$Q(V_e, p) = \frac{j_c(V_e, p)}{eW} - \frac{p - p_{no}}{\tau}, \tag{4}$$

with

$$j_e = j_s\left[\exp\left(\frac{V_e}{V_T}\right) - 1\right] + j_r\left[\exp\left(\frac{V_e}{2V_T}\right) - 1\right], \tag{5}$$

$$j_c = M j_{sc} + \beta M j_s\left[\exp\left(\frac{V_e}{V_T}\right) - 1\right] + \frac{V_i - V_e}{\rho_L}, \tag{6}$$

$$M = \left[1 - \left(\frac{V_i - V_e}{V_b}\right)^3\right]^{-1}, \tag{7}$$

and

$$V_i = V - V_T \ln\left(\frac{p}{p_{n0}}\right). \tag{8}$$

$j_s$, $j_r$, and $j_{sc}$ denote the diffusion and recombination saturation current density of the $p^+$-$n^+$ junction and the saturation current density of the $n^+$-$p$ junction, respectively. $V_T$ is the thermal voltage and $\beta$ the transport factor of the $n^+$ base. $\rho_L$ and $V_b$ denote the leakage resistance and the breakdown voltage of the $n^+$-$p$ junction. $p_{n0}$ is the equilibrium value of the mean-hole density, $\tau$ the lifetime of holes, and $W$ the width of the $n^-$ layer.

In order to get insight into the relevant physical processes let us consider the two device parts in more detail. In the usual operation, the $n^+$-$p$ junction of the $p^+$-$n^+$-$p$ transistor is reverse biased. Suppose that the voltage drop across the $n^+$-$p$ junction is sufficiently large so that charge carrier mul-

 

tiplication takes place by impact ionization. Then, a small fluctuation of the emitter voltage $V_e$ has the following consequences: Due to the essentially exponential dependence of the emitter current density on the emitter voltage, a fluctuation of $V_e$ causes an additional injection of holes into the $n^+$ layer. Those holes, which reach the high-field zone of the $n^+$-$p$ junction, generate electron-hole pairs which are separated due to the high electric field. The electrons move towards the $p^+$-$n^+$ junction and induce an additional injection of holes and, consequently, an increase of $V_e$. Because of this activating property of the transistor part, the variable $V_e$ may be called an activator.

The coupling of the transistor part to the $p$-$n^-$ diode leads to a counteraction to the autocatalytic increase of $V_e$: The current fluctuation caused by the fluctuation of $V_e$ leads to an increased hole injection into the $n^-$ layer and therefore to an augmentation of both the mean-hole concentration $p$ in the $n^-$ layer and the voltage drop $V_p = V_T \ln(p/p_{n0})$ across the $p$-$n^-$ diode. Keeping the device voltage $V$ constant means that the voltage drop $V_i = V - V_p$ across the transistor decreases if $V_p$ increases. This inhibiting process in the $p$-$n^-$ diode limits the autocatalytic process and, consequently, $p$ can be viewed as inhibiting variable. This interpretation of $V_e$ and $p$, in terms of an activating and an inhibiting variable, is confirmed by a linear stability analysis of Eqs. (1) and (2).

As the device is connected to the voltage source $V_s$ via a load resistor $R_0$, a global coupling influences the device, which occurs in the following way: Consider a positive current-density fluctuation at an arbitrary position in the device that causes a corresponding fluctuation of the total current in the external circuit. This current fluctuation leads to an increment of the voltage drop across the load resistor and, consequently, to a decrease of the device voltage, because the applied total voltage

$$V_s = V + R_0 I \tag{9}$$

is constant. The total current $I$ can be calculated by integrating the current-density distribution $j_c(x,z,t)$ along the rectangular device area $l_x \times l_z$:

$$I = \int_0^{l_z} \int_0^{l_x} j_c \, dx \, dz. \tag{10}$$

As the device voltage $V$ is only time dependent but does not depend on the space coordinates, the existence of a load resistor effects a nonlocal inhibiting feedback. Note that any real voltage source has an internal resistance; we therefore have to consider $R_0$ as a sum of this internal resistance and the load resistance. By this, in a real experiment, a global coupling is still present even in the absence of a load resistor.

### III. RESULTS AND DISCUSSION

Before the numerical results are presented, consider the null clines of Eqs. (1) and (2), that are shown in Fig. 1 for two different values of $V$. They have been calculated numerically by solving the equations $q(V_e,p)=0$ and $Q(V_e,p)=0$ which determine stationary uniform states of the system. The curve defined by $q=0$ essentially represents the current-voltage characteristic of the transistor part for a uniform current-density distribution, since $\ln(p/p_{n0})$ depends linearly on the transistor voltage $V_i$ [Eq. (8)]. Similarly, the curve defined by $Q=0$ reflects the essentially exponential behavior of the current-voltage characteristic of the diode part.

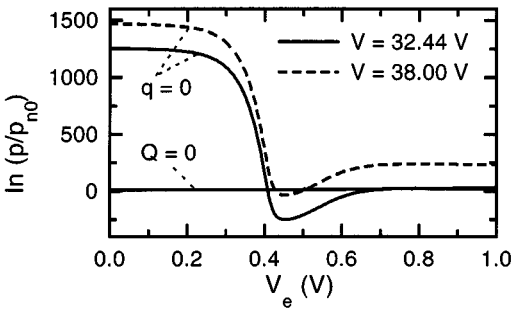


FIG. 1. Null cline system of Eqs. (1) and (2) for $V=32.44$ V (solid lines) and $V=38.00$ V (dashed lines). Other parameters: $C_e=10^{-5}$ F/cm$^2$, $j_{sc}=2\times10^{-8}$ A/cm$^2$, $j_s=1.5\times10^{-11}$ A/cm$^2$, $j_r=3\times10^{-7}$ A/cm$^2$, $l_x=l_z=0.5$ cm, $D_p=10$ cm$^2$/s, $p_{n0}=10^7$ cm$^{-3}$, $R_0=0\,\Omega$, $T=300$ K, $V_b=42$ V, $w=3\,\mu$m, $W=600\,\mu$m, $\beta=0.6$, $\rho_L=4\times10^4\,\Omega$cm$^2$, $\sigma_b=10\,(\Omega\text{cm})^{-1}$, $\tau=10\,\mu$s.

Depending on $V$ there are one, two, or three intersection points of the two curves for fixed $V$. The main effect of a variation of $V$ is a horizontal shift of the curve defined by $q=0$. The changes of the curves $Q=0$ are relatively small and cannot be resolved in Fig. 1. For all calculations presented in this paper the null cline system is bistable. We remark that Eqs. (1)–(4) have been derived for a specific model. However, it is clear from Fig. 1 that the shape of the null clines is also typical for many other physical, chemical, and biological systems of reaction-diffusion type. Therefore, we believe that the properties of spots we have found in our study are of general importance for reaction-diffusion systems.

The characteristic time constant of the inhibitor is given by the effective hole lifetime $\tau$, while the time constant $\tau_e$ of the activator is governed by the capacity $C_e$ and the resistor $\rho_c$ controlling the recharging of $C_e$: $\tau_e \approx C_e \rho_c$. In the framework of our model $\rho_c$ can be estimated from the reaction term $q$ to $\rho_c = (2V_T/j_r)\exp(-V_e/2V_T)$ [11]. This means that for low current densities and, consequently, low values of $V_e$ the activator is slower than the inhibitor, while for larger values of $V_e$ the opposite is the case. The diffusion lengths of the activator and the inhibitor are given by $L_e = \sqrt{D_e \tau_e}$ and $L = \sqrt{D_p \tau}$. For sufficiently large $V_e$ we have $L > L_e$. Thus the main features of the active medium under study are the existence of an instantaneously effective global coupling via the load resistor and a relatively slow local inhibition. The different time constants and diffusion lengths of the activator and the inhibitor lead to a competition in time and space between these variables and determine the dynamical behavior of the localized structures evolving in the system.

The simulations are based on a simplified version of the Newton-single-step integration of the finite-difference equations resulting from discretization of the Eqs. (1), (2), and (9). The spatial mesh consist of 200 by 200 grid points; spot-checks have shown that there is no qualitative differ-

ence in the results when the mesh is refined to 400 by 400 points.

First, we present results obtained by using homogeneous Neumann boundary conditions for both variables, i.e., $\partial V_e/\partial x(x=0,l_x)=\partial V_e/\partial z(z=0,l_z)=0$ and $\partial p/\partial x(x=0,l_x)=\partial p/\partial z(z=0,l_z)=0$. While for low values of $V_s$ the spatially uniform state defined by $q=0$ and $Q=0$ is stable, for sufficiently large values of $V_s$ autocatalytic charge carrier multiplication takes place and a localized structure in the form of a current-density filament develops from the spatially uniform state. Since the spatially uniform state becomes unstable with respect to fluctuations with the longest possible wavelength, the filament develops near one of the four corners of the rectangular domain. The same result is obtained when we start the calculation for a given $V_s$ with all mesh points set to zero except for an area of 25 by 25 mesh points in the center of the domain set to $V_e=0.83$ V and $p=1.34\times10^{18}$ cm$^{-3}$. In this case, the cylindrically shaped initial structure deforms to a localized structure and simultaneously moves to one of the corners of the domain.

Since the chosen Neumann boundary conditions act as a mirror, we may consider the filament in the corner as a quarter of a stationary spot the center of which is just the corner of the domain. With increasing voltage $V_s$ the width and the amplitude of this spot increase. When a certain threshold is reached, the static spot transforms to a spot with width and amplitude oscillating in antiphase. Figure 2(a) shows a series of four gray-scale diagrams of the activator distribution $V_e$. For the sake of clarity the entire spot was reconstructed. Dark regions correspond to regions where $V_e$ and correspondingly the current density $j_e$ are large. Obviously, in the course of time the spot is alternately deformed elliptically along the $x$ and $z$ axes. Thereby and by the additional appearance of antiphase amplitude oscillations, fluctuations of the total current are eliminated as imposed by the global coupling. The profiles shown in Fig. 2(b) illustrate that the spot width along the $x$ axis has a maximum at $t_1$ and a minimum at $t_3$ which coincides with a maximum elongation along the $z$ axis. For maximum spot elongations, the spot amplitude in the center, $V_e(x=0,z=0,t)$, has a minimum and vice versa, reflecting the antiphase oscillations. The finite value of the global coupling allows small oscillations of the total current and the device voltage emanating from a slight mismatch between the amplitude and width oscillations. Figure 2(c) shows the time series of the device voltage $V(t)$. The minima (maxima) of $V(t)$ correspond to maxima (minima) in the total current $I(t)$ and coincide with maximal (minimal) spot elongations along one of the two symmetry axes. The amplitude of this oscillation as well as the amplitude of the width and the height oscillation in the spot center increase monotonously from zero with increasing $V_s$; this and the finite value of the oscillation period at the bifurcation point indicate a supercritical Hopf bifurcation.

For sufficiently large width and amplitude oscillations, the filament detaches from the corner and starts traveling along the boundary of the domain. Figure 3 shows a series of activator and inhibitor distributions at different stages of the motion. From these diagrams it is obvious that the slow inhibitor has an extended tail following the activator distribution. However, there is also a small inhibitor precursor running in front of the activator. This precursor is important when the filament reaches the corner of the domain. Because of the interaction of the filament with its mirror image the inhibiting precursor hinders the activator to continue its free motion and effects a deceleration of the filament; this finally results in a reflection of the filament by the corner. Thus, the filament performs a periodic traveling motion between two corners of the domain with a maximum velocity of about 50–100 m/s.

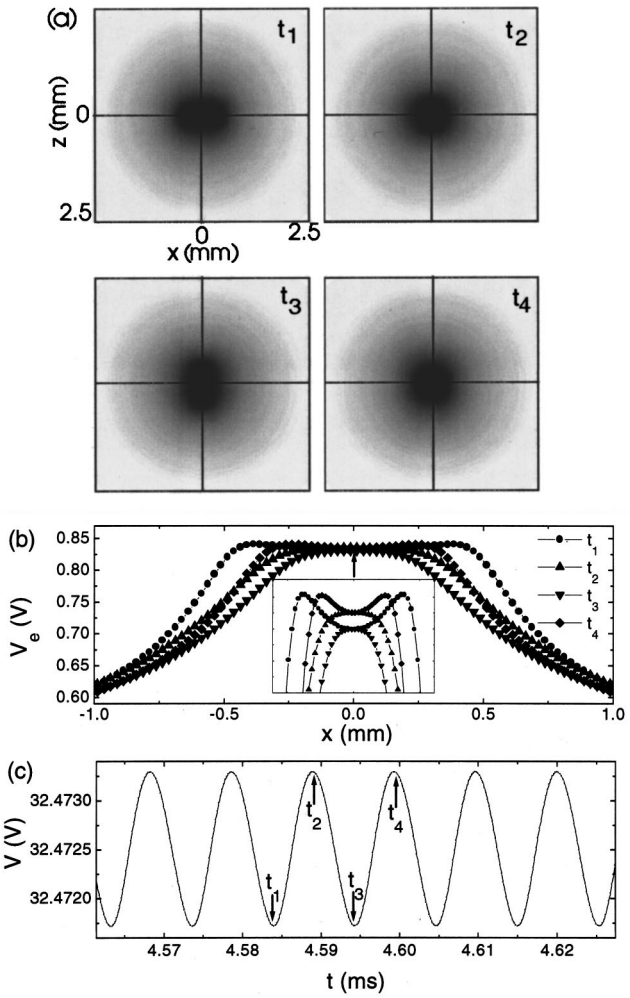


FIG. 2. Oscillating spot that is alternately deformed elliptically along the two symmetry axes defined by the domain boundary. (a) Gray-scale diagrams of the activator distribution $V_e$ at four different moments. The lower right quarter of each diagram represents the domain, the other quarters have been added. At $t_1$ and $t_3$ the elongation along the $x$ and the $z$ axis has a maximum, respectively, at $t_2$ and $t_4$ the spot width has a minimum. (b) Profiles of the activator distribution $V_e$ along the $x$ axis at the center of the spot corresponding to the diagrams shown in (a). (c) Time series of the device voltage $V(t)$. The maximum and minimum spot elongations correspond to local minina and maxima of $V(t)$, respectively. Parameters as in Fig. 1 but $V_s=1700$ V and $R_0=1$ k$\Omega$.

Again it is instructive to use the symmetry properties imposed on the system by the Neumann boundary conditions for some further considerations: In doing so, the transition from the filament oscillating near the corner to a traveling filament appears to be a splitting process of the oscillating spot into two spots that start traveling in opposite directions

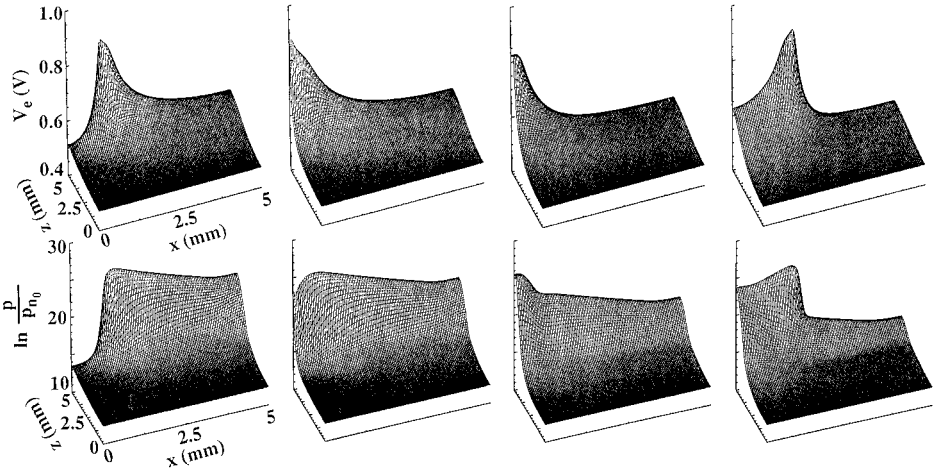


FIG. 3. Traveling spot being reflected by the corners of the domain resulting in a periodic motion. Upper (lower) diagrams refer to the activator $V_e$ (inhibitor $p$) distribution; parameters as in Fig. 1 but $V_s=1800$ V and $R_0=1$ kΩ; $t=2.1704$, 2.1786, 2.2014, 2.2278 ms (from left to right).

after the division. Therefore, the filament traveling between the corners (Fig. 3) can be viewed as half of a spot that collides with another spot (its mirror image) when it reaches the domain corner [Fig. 4(a)]. As both spots are mirror images some fundamental degrees of freedom of motion as, e.g., an antiphase amplitude oscillation of the two colliding spots, which might result in an extinction of one of the colliding spots, are excluded. Consequently, a collision of the two spots is unavoidable. Thus Neumann boundary conditions provide ideal conditions to study collision processes of localized structures.

These numerical results are confirmed by a stability analysis of the radially symmetrical spot. In this case, the perturbation modes can be separated into a radial part and an angular part, the latter being proportional to $\cos(n\phi)$, where $\phi$ denotes the angular and $n$ is a natural number. Typically, the most critical pertubation for a spot is the perturbation mode with $n=0$ (e.g., Refs. [6,7,10]). This perturbation mode would lead to a radially symmetrical widening or narrowing of the spot accompanied by a corresponding variation of the total current and is therefore suppressed in our system by the existence of the global inhibition. The mode with $n=1$ would lead to a traveling spot. This fluctuation cannot arise due to the mirror symmetry along the two symmetry axes imposed on the system by the applied Neuman boundary conditions. The perturbation mode with $n=2$ just reflects a fluctuation that leads to an elliptically deformed spot. Such a perturbation is neither damped by the global inhibition nor by the imposed symmetry conditions and, therefore, leads to the destabilization of the spot.

With increasing parameter $V_s$ the amplitude and the width of both the activator and the inhibitor distribution grow. This is accompanied by an increase of the velocity of the traveling filament, as the effective time constant of the activator decreases with its amplitude. Hence, two consequences arise: The distance between the center of the inhibitor and the activator distribution increases, the inhibitor precursor becomes smaller, and therefore, the retardation of the filament by its mirror image becomes less effective when the filament meets the corner. Moreover, the reflection process is made more difficult by the larger inhibitor tail following the filament center. As a result a qualitatively new form of filament motion appears: The reflection of the filament at the domain corner transforms into a deflection of the filament by 90° [Fig. 4(b)]. As the deflection occurs every time the filament meets a corner, a circlelike periodic motion of the filament along the domain boundary sets in.

Partly similar properties of traveling localized structures have been found by Krischer and Mikhailov [7] and by Schimansky-Geier *et al.* [8]. The former pointed out that the existence of a global coupling can lead to a suppression of a width oscillation (see also Refs. [13,14]) and, instead, a direct bifurcation of a standing to a traveling spot takes place when the inhibitor time constant is increased. Our simula-

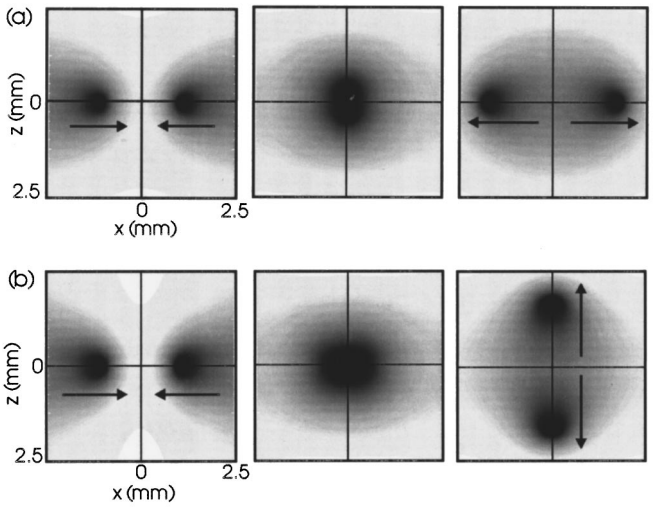


FIG. 4. Gray-scale diagrams of the activator distribution $V_e$ of colliding spots at three different moments. The lower right quarter of each diagram represents the domain. (a) Reflection of two colliding spots, $V_s=1800$ V, $t=2.1703$, 2.2014, 2.2278 ms. (b) Deflection of two colliding spots vertically to the impact direction, $V_s=2600$ V, $t=4.3722$, 4.3988, 4.4128 ms. Other parameters as in Fig. 1 but $R_0=1$ kΩ.

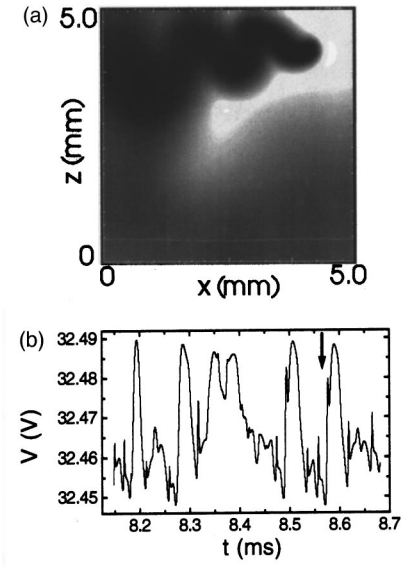


FIG. 5. (a) Gray-scale diagram of the inhibitor distribution $\ln(p/p_{n0})$ in the case of Dirichlet boundary conditions for $V_e$. (b) Appertaing irregular time series $V(t)$; the arrow indicates the time the distribution shown in (a) belongs to. Parameters as in Fig. 1 but $V_s=2600$ V, $R_0=1$ k$\Omega$, $\tau=100$ $\mu$s, $V_e=0.63$ V at the domain boundary.

tions reveal that the mode leading to a single traveling spot can be suppressed by symmetry conditions imposed on the system, so that a static spot may transform to an elliptically oscillating spot by increasing the bifurcation parameter $V_s$, that in turn transforms to two traveling spots via a splitting process of the elliptically oscillating spot.

Finally, we discuss some peculiarities that appear when we use Dirichlet boundary conditions for the activator $V_e$, which are suggested by some experimental results in the one-dimensional case [12]. For increasing parameter $V_s$ we again find a traveling filament oscillating periodically between two corners and transforming into a filament that performs a regular circlelike motion along the domain boundary. However, while in the case of Neumann boundary conditions a further increase of $V_s$ leads to a broadening of the filament and an increase of the traveling velocity, in the case of Dirichlet boundary conditions the traveling motion becomes more complicated, as indicated in Fig. 5(a), where a snapshot of the inhibitor distribution is shown. As the inhibitor relaxes very slowly, the filament motion is recorded in the tail of the inhibitor distribution. Obviously, the filament travels in a wavelike motion. When the filament reaches the corner it can be deflected. However, sometimes it is also trapped there, i.e., it performs a circlelike motion near the corner. The radius of this circle is typically of the order of 0.5 mm. After having performed several rotations, the number of which varies statistically, the filament continues its traveling motion to the next corner. It may also happen that the amplitude of the wavy motion becomes so large that the filament changes its direction between two corners. This complicated spatiotemporal behavior is based on the interplay between the domain boundary with the fixed value for $V_e$ that tends to fix the filament in a certain distance of the domain boundary [12] and the delayed reaction of the inhibitor with respect to activator fluctuations. The complex motion is accompanied by an irregular time series $V(t)$ of the device voltage as shown in Fig. 5(b). Remarkably enough, similar oscillations have been observed in a recent experiment on a two-dimensional multilayered diode. It is a challenge to supply experimental evidence that these oscillations are caused by irregular spatiotemporal filament motions as suggested by the numerical results.

We thank C. Schenk for carrying out the stability analysis. The support from the HLRZ, Jülich providing CPU time on the Paragon, and financial support from the Deutsche Forschungsgemeinschaft is gratefully acknowledged.

[1] K. J. Lee and H. L. Swinney, Phys. Rev. E **51**, 1899 (1995).
[2] R. Imhibl, Prog. Surf. Sci. **44**, 185 (1993).
[3] E. Ammelt, D. Schweng, and H.-G. Purwins, Phys. Lett. A **173**, 348 (1993).
[4] W. Breazeal, K. M. Flynn, E. G. Gwinn, Phys. Rev. E **52**, 1503 (1995).
[5] *Nonlinear Dynamics and Pattern Formation in Semiconductors and Devices*, edited by F.-J. Niedernostheide (Springer, Berlin, 1995), and references cited therein.
[6] T. Ohta, M. Mimura, and R. Kobayashi, Physica D **34**, 115 (1989).
[7] K. Krischer and A. Mikhailov, Phys. Rev. Lett. **73**, 3165 (1994).
[8] L. Schimansky-Geier, M. Mieth, H. Rosé, and H. Malchow, Phys. Lett. A **207**, 140 (1995).
[9] F.-J. Niedernostheide, M. Or-Guil, and M. Kleinkes, in *Self-Organization in Activator-Inhibitor-Systems: Semiconductors, Gas-Discharge and Chemical Active Media*, edited by H. Engel *et al.* (W und T-Verlag, Berlin, 1996), pp. 16–21.
[10] B. S. Kerner and V. V. Osipov, *Autosolitons* (Kluwer, Dordrecht, 1994).
[11] F.-J. Niedernostheide, B. S. Kerner, and H.-G. Purwins, Phys. Rev. B **46**, 7559 (1992).
[12] F.-J. Niedernostheide, M. Ardes, M. Or-Guil, and H.-G. Purwins, Phys. Rev. B **49**, 7370 (1994).
[13] F.-J. Niedernostheide, R. Dohmen, H. Willebrand, B. S. Kerner, and H.-G. Purwins, Physica D **69**, 425 (1993).
[14] R. Woesler, P. Schütz, M. Bode, M. Or-Guil, and H.-G. Purwins, Physica D **91**, 376 (1996).